Journal of Molecular Catalysis A: Chemical 334 (2011) 52–59

Contents lists available at ScienceDirect

Journal of Molecular Catalysis A: Chemical

journal homepage: www.elsevier.com/locate/molcata

In situ anion-exchange synthesis and photocatalytic activity of $Ag_8W_4O_{16}$/AgCl-nanoparticle core–shell nanorods

Xuefei Wang [a], Shufen Li [a], Huogen Yu [a,b,*], Jiaguo Yu [b,**]

[a] Department of Chemistry, School of Science, Wuhan University of Technology, Wuhan 430070, PR China
[b] State Key Laboratory of Advanced Technology for Material Synthesis and Processing, Wuhan University of Technology, Wuhan 430070, PR China

ARTICLE INFO

Article history:
Received 9 September 2010
Received in revised form 19 October 2010
Accepted 22 October 2010
Available online 30 October 2010

Keywords:
Ion-exchange
AgCl nanoparticles
Core–shell nanostructures
Visible-light activity

ABSTRACT

Usually, it is difficult to get small AgCl nanoparticles by a conventional aqueous solution route owing to their high nucleation and growth rate. In this study, AgCl nanoparticles with a diameter of less than 30 nm were uniformly coated on the surface of $Ag_8W_4O_{16}$ nanorods to form $Ag_8W_4O_{16}$/AgCl-nanoparticle core–shell heterostructures by a simple *in situ* anion-exchange route. It was found that the ion exchange reaction between Cl^- and WO_4^{2-} ions was preferable to occur on the surface of $Ag_8W_4O_{16}$ nanorods rather than in the bulk solution, resulting in the formation of core–shell nanorods. The AgCl shell layer could be easily controlled by adjusting the concentration of NaCl solution. With increasing NaCl concentration, more $Ag_8W_4O_{16}$ phase in the core transferred into AgCl-nanoparticle shell layer while the total size of the core–shell nanorods almost remained unchanged. The photocatalytic activity experiments of methyl orange aqueous solution under fluorescence light irradiation indicated that the AgCl nanoparticles coated on the surface of $Ag_8W_4O_{16}$ nanorods, which could be readily separated from a slurry system after photocatalytic reaction, exhibited a much higher photocatalytic activity than the bulk AgCl photocatalyst.

1. Introduction

One-dimensional (1D) nanostructured materials, representing a group of ideal building blocks for the bottom-up assembly of integrated electronic and photoelectronic devices, have attracted considerable attention due to their unique physical and chemical properties [1–5]. Especially, the 1D core–shell heterostructured materials have recently become of particular interest as their functions can be easily tuned by adjusting their core and shell with different materials [6–12]. Usually, the template-directed route has been widely used to prepare various 1D core–shell nanostructures [6,7]. In this case, the shell component is directly coated on the surface of 1D core template to form a core–shell structure by various strategies. In order to prepare a uniform shell on the surface of the core template, the template-directed method requires the excellent compatibility between the different core and shell materials. In fact, the conventional template-directed method usually results in incomplete coverage, different thickness of shell and weak interactions between the core and shell. Therefore, it still remains a major challenge to develop a facile and effective route for the preparation of 1D core–shell heterostructures.

In addition to conventional oxide semiconductor photocatalysts [13–19], recently, silver halides have been widely investigated and applied as a highly efficient visible-light photocatalysts [20–25]. Huang et al. reported that Ag@AgCl photocatalyst showed highly efficient and stable for the degradation of methyl orange under the visible-light irradiation [20]. Kakuta et al. found that the AgBr was not destroyed by successive UV irradiation after the formation of Ag^0 species in the early stage of the irradiation [22]. Hu et al. also reported the high efficiency and stability of Ag–AgI photocatalyst supported on mesoporous alumina for the photodegradation of toxic pollutants under visible-light irradiation [21]. All these results suggested that the silver halides could be a highly efficient and promising photocatalyst for the degradation of various organics. However, almost all of the present studies were focused on the silver halides with a size of larger than several hundreds nanometers and seldom works have been carried out on the preparation of nano-scale silver halides, especially the AgCl nanoparticles with a diameter of less than 30 nm [26–28]. One of the most possible reasons is the difficulty for its synthesis owing to its rapid nucleation and growth in aqueous solution. It is highly desirable to develop a new and facile strategy for the preparation of nano-scale silver halide photocatalysts.

* Corresponding author at: Department of Chemistry, School of Science, Wuhan University of Technology, Wuhan, PR China. Tel.: +86 27 87871029; fax: +86 27 87879468.
** Corresponding author. Tel.: +86 27 87871029; fax: +86 27 87879468.
E-mail addresses: yuhuogen@yahoo.cn (H. Yu), jiaguoyu@yahoo.com (J. Yu).

1381-1169/$ – see front matter © 2010 Elsevier B.V. All rights reserved.
doi:10.1016/j.molcata.2010.10.022

Usually, the photocatalytic activity of a sample is strongly depended on its size and specific surface area. It is expected that the photocatalytic performance of AgCl can be greatly improved by decreasing its particles size. However, conventional powdered photocatalysts have a serious limitation—the need for post-treatment separation in a slurry system after photocatalytic reaction. In addition, the nanosized powders have a strong tendency to agglomerate into larger particles, resulting in the decrease of their photocatalytic performance. Continuing efforts have been made to develop alternate methods to prepare the highly active photocatalysts, which can be readily separated after the photocatalytic reaction. In this work, the AgCl nanoparticles were uniformly coated on the surface of $Ag_8W_4O_{16}$ nanorods to form $Ag_8W_4O_{16}$/AgCl-nanoparticle core–shell 1D heterostructures. By combination of the nano-scale AgCl particles and the micro-scale $Ag_8W_4O_{16}$ nanorods, it is expected that the obtained core–shell composite heterostructures not only exhibit high photocatalytic activity but also can be easily separated from a slurry system and re-used after photocatalytic reaction. The $Ag_8W_4O_{16}$/AgCl-nanoparticle core–shell nanorods were prepared by a two-step solution-phase route. The first step was to prepare 1D $Ag_8W_4O_{16}$ nanorods, and the second was to coat AgCl nanoparticles on the surface of $Ag_8W_4O_{16}$ nanorods by an *in situ* ion-exchange reaction in a NaCl aqueous solution. The effects of the NaCl concentration on the morphology, composition and phase structure of the core–shell nanostructures were investigated and discussed. The photocatalytic activities of the $Ag_8W_4O_{16}$/AgCl-nanoparticle core–shell nanorods were evaluated by photocatalytic decolorization of methyl orange aqueous solution under fluorescence light irradiation.

2. Experimental

All reagents are analytical grade supplied by Shanghai Chemical Reagent Ltd. (PR China) and used as received without further purification.

2.1. Preparation of precursor $Ag_8W_4O_{16}$ nanorods

The starting aqueous solutions of $AgNO_3$ (0.01 mol L^{-1}) and Na_2WO_4 (0.005 mol L^{-1}) were first prepared. The synthesis of $Ag_8W_4O_{16}$ nanorods were achieved by a simple precipitation reaction between Ag^+ and WO_4^{2-} ions in distilled water. In a typical synthesis, 50 ml of $AgNO_3$ aqueous solution was poured into 50 ml of Na_2WO_4 aqueous without stirring. After the reaction solution was incubated at room temperature for 12 h, the light yellow precipitate was collected, rinsed with distilled water, and dried at room temperature to obtain $Ag_8W_4O_{16}$ nanorods.

2.2. Preparation of $Ag_8W_4O_{16}$/AgCl-nanoparticle core–shell nanorods

The synthesis of $Ag_8W_4O_{16}$/AgCl-nanoparticle core–shell nanorods were achieved by an *in situ* anion-exchange reaction of $Ag_8W_4O_{16}$ nanorods in NaCl aqueous solution in a dark condition. Initially, 0.1 g of $Ag_8W_4O_{16}$ nanorods were added into a 200 ml NaCl solution without stirring. The NaCl concentration was controlled to be 0, 0.1, 0.5, 1 and 500 mM, respectively. After the reaction solution was incubated at room temperature for 6 h, the precipitate was collected, rinsed with distilled water, and dried at 60 °C to obtain $Ag_8W_4O_{16}$/AgCl-nanoparticle core–shell nanorods.

2.3. Preparation of N-doped TiO_2

N-doped TiO_2 (N-TiO_2) was prepared as follows: 17 mL of tetrabutylorthotitanate was added into an $NH_3{\cdot}H_2O$ solution (NH_3 = 0–10 wt%) under stirring. After stirring for another 1 h, the suspension solution was aged at room temperature (25 °C) for 24 h. The resulted suspension was filtrated, washed with distilled water for 4 times and dried at 60 °C for 6 h, and then was calcined at 500 °C for 2 h to obtain N-TiO_2. It was found that when the concentration of NH_3 was controlled to be 1 wt%, the obtained N-TiO_2 showed the highest photocatalytic activity under the fluorescence light irradiation. Thus, in this study, the N-TiO_2 prepared from the 1 wt% of NH_3 solution was used as the reference in this study.

2.4. Characterization

X-ray diffraction (XRD) patterns were obtained on a Rigaku Ultima III X-ray diffractometer (Japan) using Cu Kα radiation. Morphological analysis was performed by an S-4800 field-emission scanning electron microscope (FE-SEM, Hitachi, Japan) with an acceleration voltage of 10 kV. UV–vis absorption spectra were obtained using a UV-visible spectrophotometer (UV-2550, SHIMADZU, Japan). X-ray photoelectron spectroscopy (XPS) measurements were done on a KRATOA XSAM800 XPS system with Mg Kα source. All the binding energies were referenced to the C 1s peak at 284.8 eV of the surface adventitious carbon. Nitrogen adsorption–desorption isotherms were obtained on an ASAP 2020 (Micromeritics Instruments, USA) nitrogen adsorption apparatus. The sample was degassed at 60 °C prior to BET measurements. The Brunauer–Emmett–Teller (BET) specific surface area (S_{BET}) was determined by a multipoint BET method using the adsorption data in the relative pressure (P/P_0) range of 0.05–0.25.

2.5. Photocatalytic activity

The evaluation of photocatalytic activity of the prepared samples for the photocatalytic decolorization of methyl orange (MO) aqueous solution was performed at ambient temperature. 0.05 g of the prepared sample was dispersed into 10 ml of MO solution (15 mg/L) in a culture dish with a diameter of ca. 5 cm. A 55 W fluorescence lamp was used at a light source. The average light intensity striking the surface of the reaction solution was about 14,700 lx, as measured by a luxmeter (ZDS-10, Shanghai). The concentration of MO was determined by an UV-visible spectrophotometer (UV-2550, SHIMADZU, Japan). After visible-light irradiation for some time, the reaction solution was centrifuged to measure the concentration of MO. As for the methyl orange aqueous solution with low concentration, its photocatalytic decolorization is a pseudo-first-order reaction and its kinetics may be expressed as $\ln(c_0/c) = kt$, where k is the apparent rate constant, and c_0 and c are the methyl orange concentrations at initial state and after irradiation for t min, respectively [29,30].

3. Result and discussion

3.1. Morphology and phase structures of the precursor $Ag_8W_4O_{16}$ nanorods

The precursor of $Ag_8W_4O_{16}$ nanorods can be easily synthesized by simply mixing $AgNO_3$ and Na_2WO_4 aqueous solutions without stirring at ambient temperature (ca. 25 °C) [31]. When $AgNO_3$ aqueous solutions were poured into Na_2WO_4 solutions, a white suspension was formed immediately and the precipitate showed a cotton-like product. After aging for 12 h, the product was changed from white color to light yellow. SEM image (Fig. 1a) clearly shows that the light yellow precipitate is composed of many nanorods with a diameter of 30–100 nm and a length of ca. 1 μm. According to XRD result (Fig. 2a), these nanorods can be attributed to $Ag_8W_4O_{16}$ (JCPDS no. 70-1719) with an orthorhombic structure. To further observe the surface morphology of the $Ag_8W_4O_{16}$ nanorods, a higher magnification SEM image is shown in Fig. 1b. It is clear that

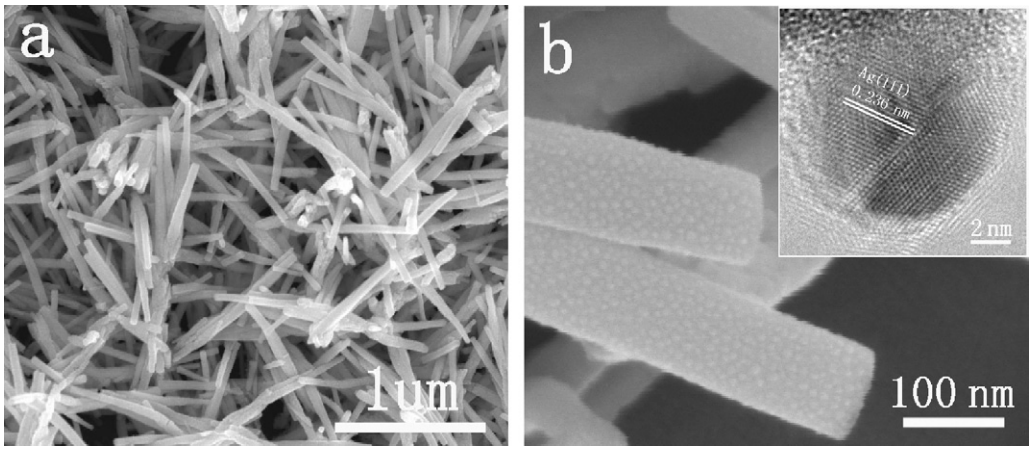

Fig. 1. SEM images of the precursor $Ag_8W_4O_{16}$ nanorods (inset in b shows a HRTEM image of a nanoparticle coated on the surface of $Ag_8W_4O_{16}$ nanorods.)

many very small nanoparticles with a diameter of 5–10 nm are uniformly coated on the surface of the $Ag_8W_4O_{16}$ nanorods. By HRTEM analysis (inset in Fig. 1b), those nanoparticles can be ascribed to metal Ag. The possible reason for the formation of Ag nanoparticles is that $AgNO_3$ is photosensitive and easy to form Ag during the synthesis and aging of $Ag_8W_4O_{16}$ nanorods. In addition, a small part of $Ag_8W_4O_{16}$ is possibly decomposed to form metal Ag during aging as most of the Ag-based materials are photosensitive and instable. As a consequence, it is not surprising that no Ag diffraction peaks can be found in Fig. 2a due to limited amount of metal Ag with very small size and uniform distribution.

3.2. Morphology and microstructures of the $Ag_8W_4O_{16}$/AgCl-nanoparticle core–shell nanorods

The prepared $Ag_8W_4O_{16}$ nanorods are used as the precursor for the preparation of $Ag_8W_4O_{16}$/AgCl-nanoparticle core–shell nanorods. To investigate the effect of NaCl solution on the surface morphology and crystalline phase of the core–shell nanorods, the NaCl concentration is varied from 0.1 mM to 500 mM. Fig. 3a and b shows the SEM images of the core–shell sample obtained from a 0.1 mM NaCl solution. It can be seen that many nanoparticles with a diameter of 5–15 nm are uniformly coated on the surface of $Ag_8W_4O_{16}$ nanorods. The corresponding XRD pattern (Fig. 2b) shows that these nanoparticles can be ascribed to AgCl

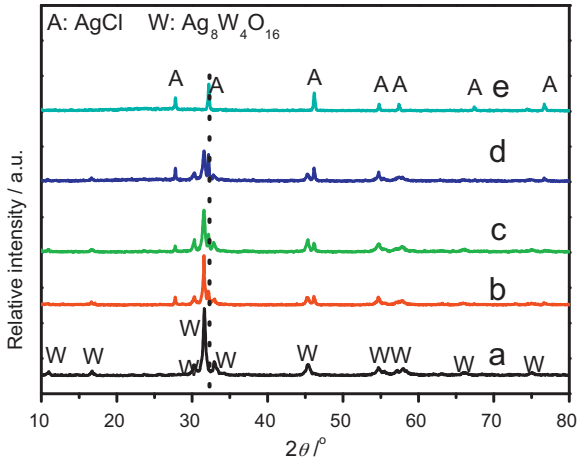

Fig. 2. XRD patterns of the $Ag_8W_4O_{16}$/AgCl-nanoparticle core–shell nanorods obtained in NaCl aqueous solutions: (a) 0 mM; (b) 0.1 mM; (c) 0.5 mM; (d) 1 mM; (e) 500 mM.

phase (JCPDS no. 31-1238) with a cubic structure, indicating the formation of $Ag_8W_4O_{16}$/AgCl-nanoparticle core–shell nanorods. The core–shell nanostructure can also be observed by TEM, as shown in the inset in Fig. 2b. Unfortunately, it is impossible to further analyze the Ag and AgCl nanoparticles on the shell layer by HRTEM analysis owing to the instability of AgCl phase under the irradiation of high-energy electron beam. With increasing NaCl concentration to 0.5 mM, more AgCl nanoparticles with a larger size of 7–20 nm are formed on the surface of $Ag_8W_4O_{16}$ nanorods (Fig. 3c and d). When the NaCl concentration is increased to 1 mM, the size of AgCl nanoparticles is further increased to 10–30 nm (Fig. 3f). However, the $Ag_8W_4O_{16}$/AgCl-nanoparticle core–shell nanorods clearly become shorten. This can be ascribed to the fact that increasing NaCl concentration produces a faster *in situ* ion-exchange reaction between $Ag_8W_4O_{16}$ and Cl^-, resulting in the partial destroys of core–shell nanorods. Actually, the composite nanorods are completely destroyed when the NaCl concentration is increased to 500 mM and only micro-scale AgCl particles is formed (Fig. 3g). The above fact strongly suggests that the size of AgCl nanoparticles can be easily controlled by adjusting the NaCl concentration to control the formation rate of AgCl phase.

Fig. 4 shows the UV–vis spectra of the $Ag_8W_4O_{16}$/AgCl-nanoparticle core–shell nanorods obtained in various NaCl solutions. As for the precursor $Ag_8W_4O_{16}$ nanorods, an absorption shoulder at 400–600 nm is found in addition to the band gap absorption at 400 nm. Based on the SEM and HRTEM analysis (Fig. 1), the visible-light absorption at 400–600 nm can be attributed to the localized surface plasmon resonance of Ag nanoparticles coated on the surface of $Ag_8W_4O_{16}$ nanorods [20]. After the $Ag_8W_4O_{16}$ nanorods are put into 0.1 mM NaCl solution for 6 h, the plasmon resonance absorption peak of metal Ag is partially overlapped with the Ag/AgCl absorption in the visible-light region. With increasing NaCl concentration to 1 mM, an obvious enhanced absorption in the visible-light regions is observed for the obtained $Ag_8W_4O_{16}$/AgCl-nanoparticle core–shell nanorods. Moreover, the plasmon resonance absorption peak shifts to a longer wavelength from ca. 480 nm to ca. 590 nm. It is well known that the absorption peak of surface plasmon resonance of Ag nanoparticles is greatly influenced by their shape, size, composition and dielectric environment [32,33]. In this study, as only AgCl phase is formed and $Ag_8W_4O_{16}$ is partially decomposed when $Ag_8W_4O_{16}$ nanorods are added into NaCl solution to form core–shell nanorods, the shift of the plasmon resonance absorption peak can be mainly attributed to the change of its dielectric environment. When the NaCl concentration increases to 500 mM, the resulted sample shows a wide absorption in the whole UV–vis regions. This is ascribed to the fact that the obtained sample is Ag/AgCl composite phases

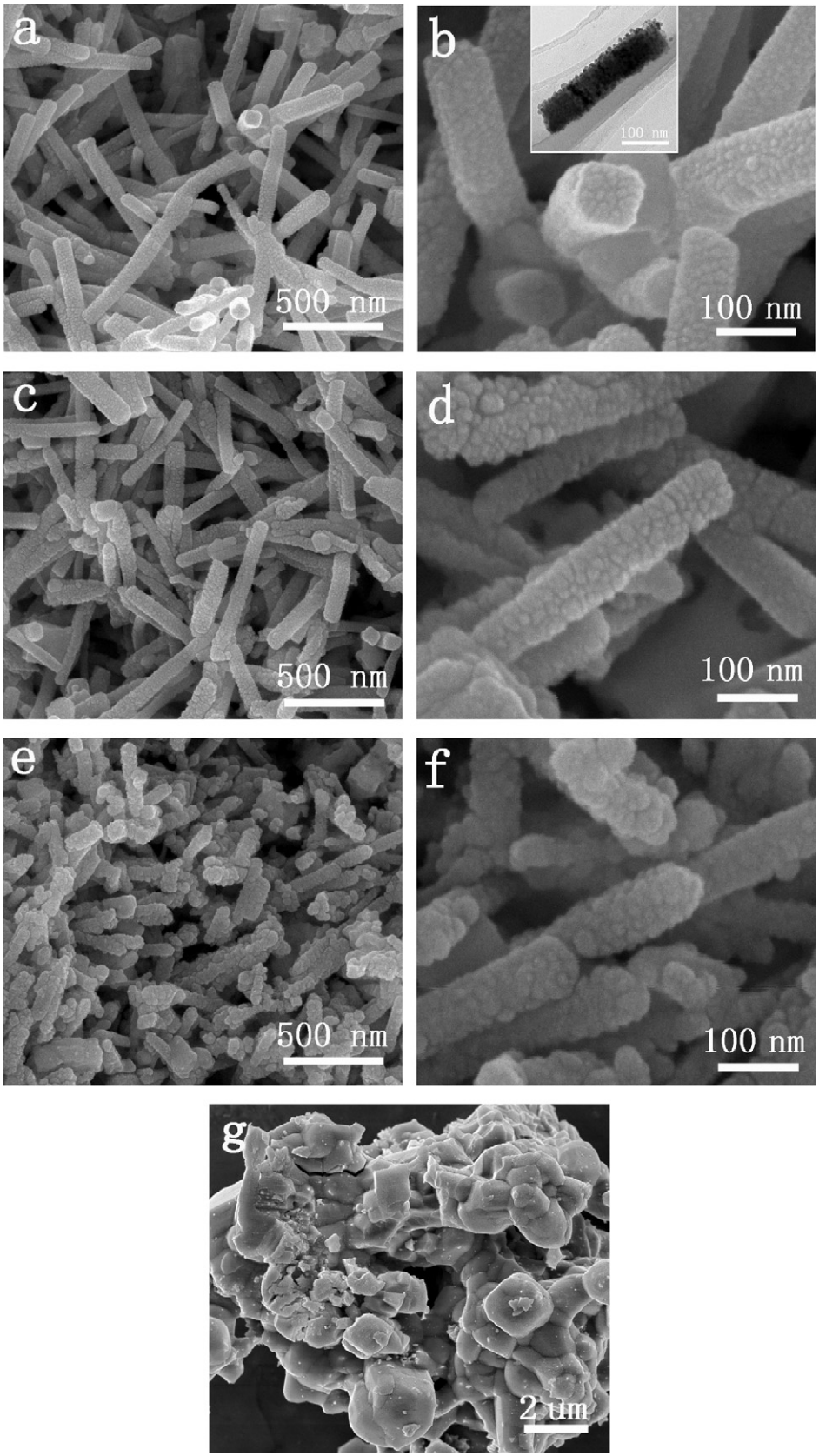

Fig. 3. SEM images of the $Ag_8W_4O_{16}$/AgCl-nanoparticle core–shell nanorods obtained in NaCl aqueous solutions: (a and b) 0.1 mM (inset in b is a corresponding TEM image); (c and d) 0.5 mM; (e and f) 1 mM; (g) 500 mM.

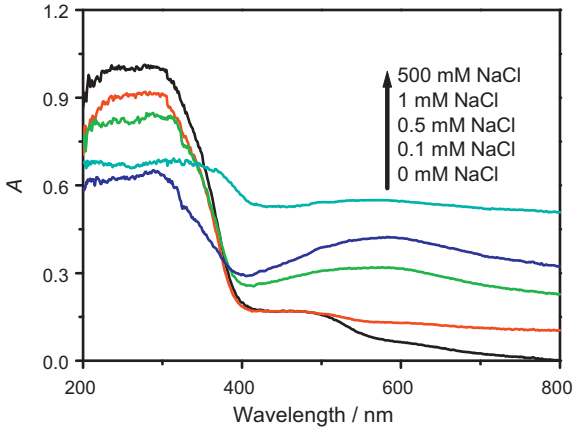

Fig. 4. UV–vis spectra of the $Ag_8W_4O_{16}$/AgCl-nanoparticle core–shell nanorods obtained in NaCl solutions.

(Fig. 2e) that shows a wide absorption as reported in the previous study [20].

The elemental compositions and chemical status of the $Ag_8W_4O_{16}$/AgCl-nanoparticle core–shell nanorods were analyzed by XPS. Compared with the precursor $Ag_8W_4O_{16}$ nanorods, a new Cl element was found in the $Ag_8W_4O_{16}$/AgCl-nanoparticle core–shell nanorods in addition to the Ag, W, O and C elements based on the XPS survey spectra (not shown here) due to the formation of AgCl phase. To investigate the chemical status of Ag element in the obtained samples, a pure AgCl was prepared by a precipitation reaction between $AgNO_3$ and NaCl solution under a dark condition and the corresponding XPS result was shown in Fig. 5A. Compared with the pure AgCl phase, a new shoulder peak of metal Ag at 369.2 eV is formed in addition to Ag^+ peak at 367.3 eV in the $Ag_8W_4O_{16}$ nanorods and $Ag_8W_4O_{16}$/AgCl-nanoparticle core–shell nanorods [25]. According to the results of curve-fitting of Ag 3d XPS spectra (Fig. 5B), the atom ratio of metal Ag to Ag^+ is calculated to be 1:2.8 for the $Ag_8W_4O_{16}$/AgCl-nanoparticle core–shell nanorods.

3.3. Formation mechanism of the $Ag_8W_4O_{16}$/AgCl-nanoparticle core–shell nanorods

In this study, it is interesting to investigate the formation mechanism of the $Ag_8W_4O_{16}$/AgCl-nanoparticle core–shell nanorods. From the XRD results (Fig. 2), with increasing NaCl concentration from 0.1 mM to 1 mM, the intensity of AgCl diffraction peak at 32.2° increases obviously while that of $Ag_8W_4O_{16}$ diffraction peak at 31.6° decreases gradually. Especially, when the NaCl concentration further increases to 500 mM, all the diffraction peaks of $Ag_8W_4O_{16}$ disappear completely and only AgCl phase is observed. This can be attributed to the fact that the formation of AgCl nanoparticles is accompanied with the dissolution of $Ag_8W_4O_{16}$ nanorods. Thus, the following reactions may occur in this study:

$$Ag_8W_4O_{16} \rightarrow 8Ag^+ + 4WO_4^{2-} \quad (1)$$

$$Ag^+ + Cl^- \rightarrow AgCl \quad (2)$$

As for reaction Eq. (1), the $Ag_8W_4O_{16}$ phase is partially dissolved in aqueous solution to form Ag^+ and WO_4^{2-} according to the precipitation–dissolution equilibrium of $Ag_8W_4O_{16}$. Subsequently, the Cl^- in NaCl solution reacts with dissolved Ag^+ to form AgCl phase by the reaction (2). Therefore, it seems that the reaction (1) occurs firstly to provide dissociative Ag^+ and then reaction (2) takes place to produce AgCl nanoparticles. If so, it is possible for us to observe many individual AgCl aggregates in the reaction solution and the size of the $Ag_8W_4O_{16}$ nanorods will have an obvious decrease due to its gradual dissolution. In this study, however,

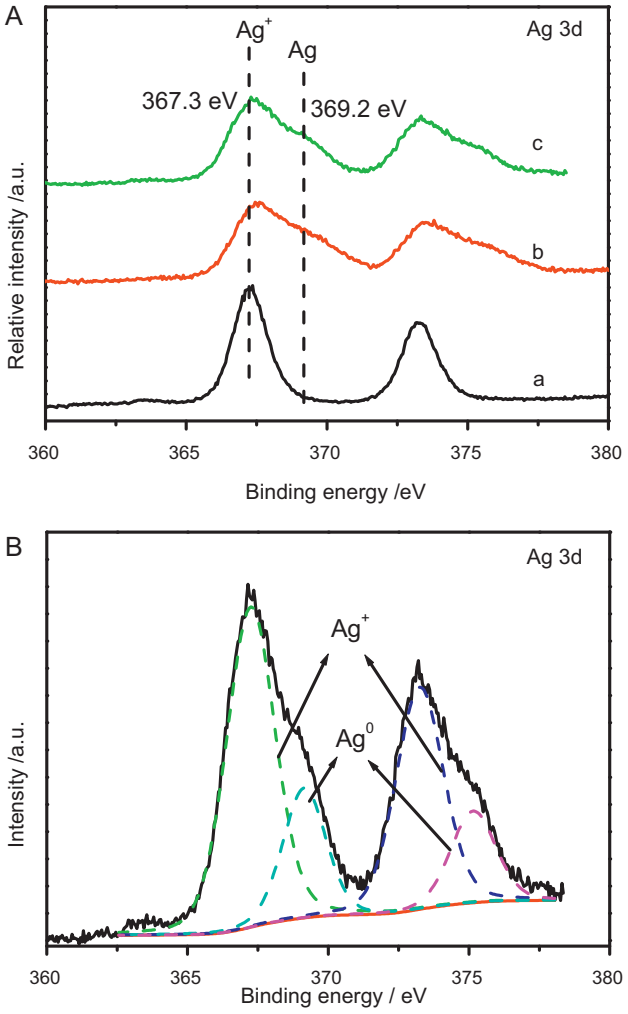

Fig. 5. (A) XPS spectra of Ag 3d for (a) pure AgCl phase; (b) $Ag_8W_4O_{16}$ nanorods; (c) $Ag_8W_4O_{16}$/AgCl-nanoparticle core–shell nanorods obtained from 0.1 mM of NaCl solution. (B) XPS spectrum of Ag 3d for the $Ag_8W_4O_{16}$/AgCl-nanoparticle core–shell nanorods obtained from 0.1 mM of NaCl solution.

after incubation of $Ag_8W_4O_{16}$ nanorods in NaCl aqueous solutions, the size of the $Ag_8W_4O_{16}$/AgCl-nanoparticle core–shell nanorods is quiet similar to that of the precursor $Ag_8W_4O_{16}$ nanorods, as shown in Figs. 1 and 3. In addition, almost no individual AgCl aggregates can be found in addition to the $Ag_8W_4O_{16}$/AgCl-nanoparticle core–shell nanorods. The above results clearly suggest that the AgCl nanoparticles are possibly *in situ* formed on the surface of $Ag_8W_4O_{16}$ nanorods by an ion-exchange reaction of Cl^- with WO_4^{2-}. In other words, one WO_4^{2-} ion in $Ag_8W_4O_{16}$ nanorods is *in situ* replaced by two Cl^- ions and then AgCl nanoparticles are formed on the surface of $Ag_8W_4O_{16}$ nanorods, as shown in Fig. 6.

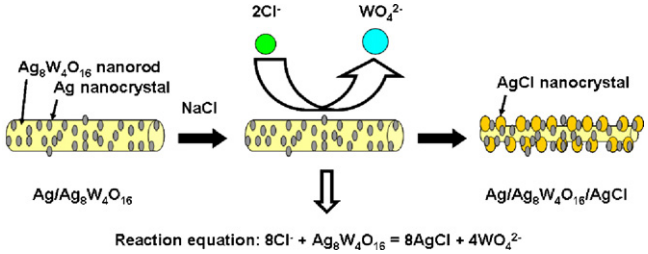

Fig. 6. Schematic illustrations for the formation mechanism of the $Ag_8W_4O_{16}$/AgCl-nanoparticle core–shell nanorods in the NaCl aqueous solutions.

In our previous study, based on the template-directed coating and *in situ* template-sacrificial reaction, we have prepared the one-dimensional TiO_2-based core–shell and hollow nanostructures in a TiF_4 solution by using vanadium oxide nanobelts as a template [10]. It was found that the coating of TiO_2 nanoparticles on the surface of the templates was accompanied with the dissolution of vanadium oxide nanobelts by HF produced during the hydrolysis of TiF_4 in the reaction solution. In this study, although the formation process of the $Ag_8W_4O_{16}$/AgCl-nanoparticle core–shell nanorods also includes the coating of AgCl shell layer and the *in situ* dissolution of $Ag_8W_4O_{16}$ core, there is an obvious difference. In the present work, the produce of AgCl shell is based on the destruction of $Ag_8W_4O_{16}$ core, namely, the $Ag_8W_4O_{16}$ core template participates in the formation of AgCl-nanoparticle shell layer. On the contrary, vanadium oxide nanobelt template did not contribute to the formation of TiO_2 shell and just acted as a template directing the growth of TiO_2 shell. Apparently, the present work is also different from the recent reported *in situ* oxidation synthesis of Ag/AgCl core–shell nanowires between Ag nanowires and $FeCl_3$ solution [8].

The above results highlight a facile ion-exchange route for the preparation of $Ag_8W_4O_{16}$/AgCl-nanoparticle core–shell nanorods. There are several obvious advantages for the application of ion-exchange route: (1) compared with the micro-scale AgCl aggregates prepared by conventional precipitation reaction, the AgCl nanoparticles with a size of less than 30 nm can be facilely prepared; (2) the size and the amount of AgCl nanoparticles can be easily controlled only by adjusting the NaCl concentration; (3) the prepared AgCl nanoparticles is preferred to coat on the surface of templates, resulting in the flexibility of synthesis methods for other core–shell nanostructures such as spheres, nanowires, nanofibers, nanotubes, etc. In fact, further investigates have being carried out.

3.4. Photocatalytic activities of the $Ag_8W_4O_{16}$/AgCl-nanoparticle core–shell nanorods

The photocatalytic performance of the $Ag_8W_4O_{16}$/AgCl-nanoparticle core–shell nanorods was evaluated by the photocatalytic decolorization of methyl orange (MO) aqueous solution under fluorescent light irradiation. For comparison, the photocatalytic activity of the typical N-TiO_2 photocatalyst was also tested under the identical experimental conditions. Fig. 7 shows the relationship between the apparent rate constants of methyl orange decolorization and the $Ag_8W_4O_{16}$/AgCl-nanoparticle core–shell nanorods prepared in various NaCl concentrations. It is found that the precursor $Ag_8W_4O_{16}$ nanorods show a very low photocatalytic activity and the corresponding apparent rate constant (k) is 0.25×10^{-3} min^{-1}. In view of the existing metal Ag nanoparticles on the surface of $Ag_8W_4O_{16}$ nanorods (Fig. 1) and its corresponding visible-light absorption at 400–550 nm (Fig. 4), the low visible-light photocatalytic activity of $Ag_8W_4O_{16}$ nanorods can be attributed to the plasmonic photocatalyst of metal Ag nanoparticles [20,33]. When the $Ag_8W_4O_{16}$ nanorods are put into 0.1 mM of NaCl solution to form $Ag_8W_4O_{16}$/AgCl-nanoparticle core–shell nanorods, the photocatalytic activity of the sample has an obvious increase and the corresponding k increases to 1.64×10^{-3} min^{-1}. With increasing NaCl concentration from 0.1 mM to 1 mM, the photocatalytic performance of the obtained core–shell nanorods further increases. When $Ag_8W_4O_{16}$ nanorods are completely transferred into AgCl phase, the photocatalytic activity of the sample reaches the highest value and the k value is 4.75×10^{-3} min^{-1}. Compared with the N-TiO_2 photocatalyst in Fig. 7, all the $Ag_8W_4O_{16}$/AgCl-nanoparticle core–shell nanorods show a much better photocatalytic performance. To exclude the effect of other factors on the photocatalytic activity of samples, the controlled experiments were designed as follows. Under dark condition with the present of various photocatalysts such as $Ag_8W_4O_{16}$ nanorods, N-TiO_2, and $Ag_8W_4O_{16}$/AgCl-nanoparticle core–shell nanorods, respectively, the concentration of MO does not change for every measurement. Similarly, illumination in the absence of photocatalyst does not result in the photocatalytic decolorization of MO. These results strongly suggest that the degradation decolorization of MO aqueous solution is caused by photocatalytic reactions under the fluorescent light irradiation.

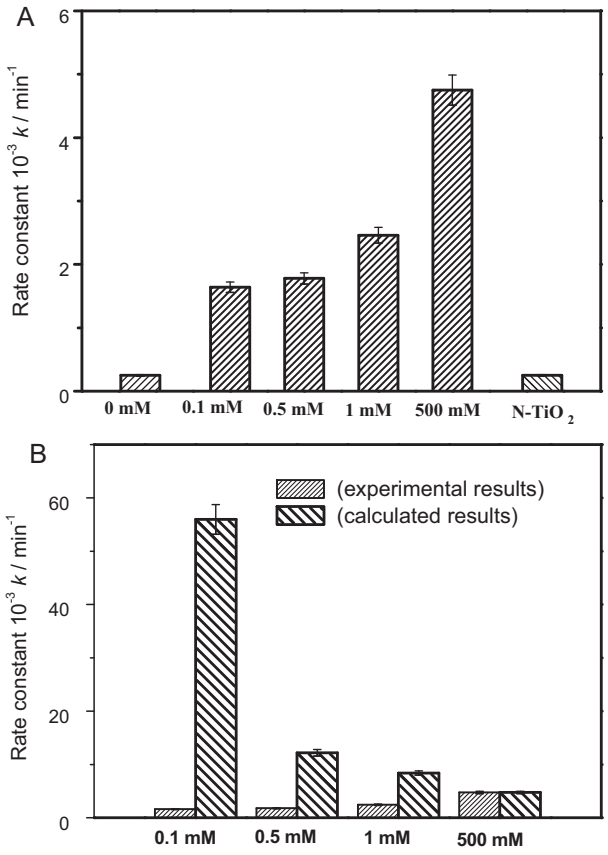

Fig. 7. (A) Photocatalytic activities of the $Ag_8W_4O_{16}$/AgCl-nanoparticle core–shell nanorods obtained in various NaCl solutions. (B) The calculated photocatalytic activity of the active component of AgCl nanoparticles (keeping the same amount of AgCl phase in the photocatalysts). For comparison, the experimental results in (A) were also shown here.

It should be pointed out that the $Ag_8W_4O_{16}$ phase shows no visible-light photocatalytic activity due to the absence of visible-light absorption (Fig. 4) and the visible-light performance of the $Ag_8W_4O_{16}$/AgCl-nanoparticle core–shell nanorods mainly arises from the active component of AgCl/Ag phases. In this study, we use 0.05 g of the $Ag_8W_4O_{16}$/AgCl-nanoparticle core–shell nanorods as the photocatalyst for every photocatalytic test. Apparently, the active component of AgCl nanoparticles coated on the surface of $Ag_8W_4O_{16}$ nanorods is far less than 0.05 g. To learn the composition of the $Ag_8W_4O_{16}$/AgCl-nanoparticle core–shell nanorods, it is supposed that all the Cl^- ions in NaCl solution are consumed completely by Ag^+ in $Ag_8W_4O_{16}$ phase to form AgCl nanoparticles and the corresponding calculated results are shown in Table 1. It is clear to seen that only 2.9 wt%, 14.6 wt% and 29.3 wt% of active components (AgCl) are present in the core–shell photocatalysts prepared from 0.1 mM, 0.5 mM and 1 mM of NaCl solutions, respectively. To compare the photocatalytic performance of AgCl nanoparticles and bulk AgCl, 0.05 g of the active component of AgCl is used as a reference to calculate the visible-light activity and the results are shown in Fig. 7b. It is clear that the AgCl nanoparticles coated on the $Ag_8W_4O_{16}$ nanorods show a much higher photocatalytic activity than the bulk AgCl prepared from 500 mM of NaCl solution. Espe-

Table 1
Phase composition, particle size of AgCl and specific surface area of the $Ag_8W_4O_{16}$/AgCl-nanoparticle core–shell nanorods prepared from various NaCl solutions.

NaCl concentration	W_{AgCl} (wt%)[a]	$W_{Ag_8W_4O_{16}}$ (wt%)[a]	D_{AgCl} (nm)[b]	S_{BET} (m^2/g)[c]
0 mM	0	100	0	7.2
0.1 mM	2.9	97.1	5–15	7.8
0.5 mM	14.6	85.4	7–020	8.3
1 mM	29.3	70.7	10-30	9.1
500 mM	100	0	>1 μm	0.5

[a] The relative contents of AgCl and $Ag_8W_4O_{16}$ are obtained from the calculation by the assumption that all the Cl^- ions in NaCl solutions are consumed to form AgCl nanoparticles.
[b] The size of the AgCl nanoparticles is obtained from SEM images.
[c] The specific surface area (S_{BET}) was determined by a multipoint BET method using the adsorption data in the relative pressure (P/P_0) range of 0.05–0.25.

cially, the sample prepared from 0.1 mM of NaCl solution shows the highest photocatalytic activity and its k reaches 56.6×10^{-3} min^{-1}. Compared with the bulk AgCl photocatalyst ($k = 4.7 \times 10^{-3}$ min^{-1}), there is a 12-time increase for the decomposition rate of MO. This can be attributed to the synthetic function of smaller AgCl nanoparticles, larger specific surface area (Table 1), well dispersed property (cotton-like suspension) in MO solution and uniform coating of AgCl nanoparticles on the surface of $Ag_8W_4O_{16}$ nanorods.

Recently, the plasmonic photocatalyst of metal Ag has been extensively investigated, especially in silver halide system. In this study, it is found that the Ag–$Ag_8W_4O_{16}$ nanorods show a low photocatalytic activity. However, once a small amount of AgCl is formed (2.9 wt%), the photocatalytic performance of the sample has a dramatic increase, as shown in Fig. 7a. Thus, the AgCl phase in this study plays a very important role for the high photocatalytic activity. As for the samples prepared from 0.5 mM to 1 mM of NaCl solution, the amount of AgCl nanoparticles has an obvious increase compared with the sample obtained from 0.1 mM of NaCl solution. However, their photocatalytic activities only show limited increase (Fig. 7a). One of the possible reasons is that the ratio of metal Ag to AgCl is a key factor that affects the photocatalytic activity in Ag–AgCl photocatalyst. Owing to limited investigations at present about the Ag–AgCl system, the visible-light photocatalytic mechanism cannot be understood fully and further investigation is needed.

As a good photocatalyst for practical applications in wastewater, a material should be easily reclaimed and re-used in addition to its high efficiency. It is clear that commercial P25 photocatalyst almost cannot be separated completely from a slurry system after photocatalytic reaction owing to its small particle size, while N-TiO_2 photocatalyst sometimes suffers from instability under repeated light irradiation and usually shows a low photocatalytic performance [34,35]. This hindered its wide applications. In this study, it was found that when the $Ag_8W_4O_{16}$/AgCl-nanoparticle core–shell nanorods were dispersed into the MO solution before irradiation with visible light, the suspension powder showed a cotton-like structure owing to their micro-scale structure, as shown in Fig. 8 (left). In this case, a clear MO solution (shown in the left cuvette) can easily be obtained from the reaction solution before centrifugation. After photocatalytic reaction, the cotton-like photocatalyst can easily be filtrated from the MO solution and then re-dispersed into the solution. As for the P25 in the MO solution, shown in Fig. 8 (right), only homogeneous suspension powder was obtained. Even after 6000-min^{-1} (rpm) centrifugation, TiO_2 nanoparticles in P25 cannot be removed completely. Moreover, compared with the usual thin-film photocatalysts, the $Ag_8W_4O_{16}$/AgCl-nanoparticle core–shell structures usually have a larger specific surface area, which is beneficial to the enhancement of photocatalytic activity. Therefore, the obtained $Ag_8W_4O_{16}$/AgCl-nanoparticle core–shell photocatalysts can be regarded as one of the ideal and novel photocatalysts for the application at industrial scales, which has been seriously impeded by the high cost for separating nanocrystal catalysts.

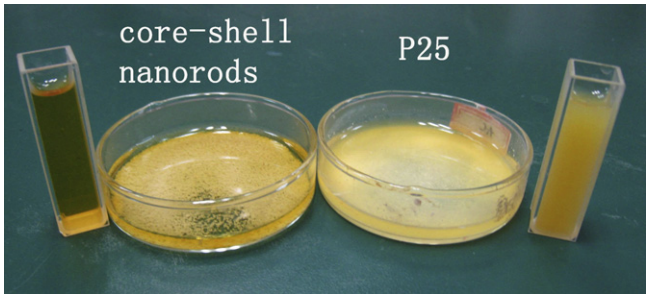

Fig. 8. The compared images of $Ag_8W_4O_{16}$/AgCl-nanoparticle core–shell nanorods (left) and P25 (right) dispersed in the MO reaction solution.

4. Conclusions

$Ag_8W_4O_{16}$/AgCl-nanoparticle core–shell nanorods were prepared by an *in situ* anion-exchange reaction between Cl^- in NaCl solution and WO_4^{2-} in $Ag_8W_4O_{16}$ nanorods. The formation of AgCl-nanoparticle shell was accompanied with the dissolution of $Ag_8W_4O_{16}$ nanorods while the total size of composite nanorods kept unchanged. The AgCl nanoparticle shell layer could be easily controlled by adjusting the NaCl concentration and more AgCl phase was produced with increasing NaCl concentration. The photocatalytic activity experiments indicated that the prepared $Ag_8W_4O_{16}$/AgCl-nanoparticle core–shell nanorods, which could be readily separated from a slurry system after photocatalytic reaction, exhibited a much higher photocatalytic activity than the bulk AgCl photocatalyst.

Acknowledgment

This work was partially supported by National Natural Science Foundation of China (20803055, 50625208, 20773097 and 20877061). This work was also financially supported by self-determined and innovative research funds of WUT (2010-1a-008).

References

[1] S. Iijima, Nature 354 (1991) 56.
[2] Z.W. Pan, Z.R. Dai, Z.L. Wang, Science 291 (2001) 1947.
[3] A.M. Morales, C.M. Lieber, Science 279 (1998) 208.
[4] J.G. Yu, J.C. Yu, W.K. Ho, L. Wu, X.C. Wang, J. Am. Chem. Soc. 126 (2004) 3422.
[5] J.G. Yu, F.R.F. Fan, S.L. Pan, V.M. Lynch, K.M. omer, A.J. Bard, J. Am. Chem. Soc. 130 (2008) 7196.
[6] L.J. Lauhon, M.S. Gudiksen, D. Wang, C.M. Lieber, Nature 420 (2002) 57.
[7] Y.J. Hwang, A. Boukai, P.D. Yang, Nano Lett. 9 (2009) 410.
[8] Y.B. Bi, J.H. Ye, Chem. Commun. (2009) 6551.
[9] H.G. Yu, J.G. Yu, B. Cheng, J. Mol. Catal. A: Chem. 253 (2006) 99.
[10] H.G. Yu, J.G. Yu, B. Cheng, S.W. Liu, Nanotechnology 18 (2007) 065604.
[11] H.G. Yu, J.G. Yu, B. Cheng, J. Lin, J. Hazard. Mater. 147 (2007) 581.
[12] T. Mokari, U. Banin, Chem. Mater. 15 (2003) 3955.
[13] H.G. Yu, H. Irie, K. Hashimoto, J. Am. Chem. Soc. 132 (2010) 6898.
[14] S.W. Liu, J.G. Yu, M. Jaroniec, J. Am. Chem. Soc. 132 (2010) 11914.
[15] R. Abe, H. Takami, N. Murakami, B. Ohtani, J. Am. Chem. Soc. 130 (2008) 7780.
[16] Z.G. Zhao, M. Miyauchi, Angew. Chem. Int. Ed. 47 (2008) 7051.
[17] H. Irie, S. Miura, K. Kamiya, K. Hashimoto, Chem. Phys. Lett. 457 (2008) 202.
[18] Y.W. Cheng, R.C.Y. Chan, P.K. Wong, Water Res. 41 (2007) 842.
[19] M. Ksibi, S. Rossignol, J.M. Tatibouet, C. Trapalis, Mater. Lett. 62 (2008) 4204.

[20] P. Wang, B.B. Huang, X.Y. Qin, X.Y. Zhang, Y. Dai, J.Y. Wei, M.H. Whangbo, Angew. Chem. Int. Ed. 47 (2008) 7931.
[21] C. Hu, T.W. Peng, X.X. Hu, Y.L. Nie, X.F. Zhou, J.H. Qu, H. He, J. Am. Chem. Soc. 132 (2010) 857.
[22] N. Kakuta, N. Goto, H. Ohkita, T. Mizushima, J. Phys. Chem. B 103 (1999) 5917.
[23] J.G. Yu, G.P. Dai, B.B. Huang, J. Phys. Chem. C 113 (2009) 16394.
[24] M.R. Elahifard, S. Rahimnejad, S. Haghighi, M.R. Gholami, J. Am. Chem. Soc. 129 (2007) 9552.
[25] Y.Z. Li, H. Zhang, Z.M. Guo, J.J. Han, X.J. Zhao, Q.N. Zhao, S.J. Kim, Langmuir 24 (2008) 8351.
[26] C.H. An, S. Peng, Y.G. Sun, Adv. Mater. 22 (2010) 2570.
[27] P. Wang, B.B. Huang, Z.Z. Lou, X.Y. Zhang, X.Y. Qin, Y. Dai, Z.K. Zheng, X.N. Wang, Chem. Eur. J. 16 (2010) 538.
[28] Y.Y. Li, Y. Ding, J. Phys. Chem. C 114 (2010) 3175.
[29] J.G. Yu, H.G. Yu, B. Cheng, X.J. Zhao, J.C. Yu, W.K. Ho, J. Phys. Chem. B 107 (2003) 13871.
[30] J.G. Yu, H.G. Yu, H.T. Guo, M. Li, S. Mann, Small 4 (2008) 87.
[31] T. George, S. Joseph, S. Mathew, Pramana-J. Phys. 65 (2005) 793.
[32] J.G. Yu, H.Z. Tao, B. Cheng, ChemPhysChem 11 (2010) 1617.
[33] Q.J. Xiang, J.G. Yu, B. Cheng, H.C. Ong, Chem. Asian J. 5 (2010) 1466.
[34] R. Asahi, T. Morikawa, T. Ohwaki, K. Aoki, Y. Taga, Science 293 (2001) 269.
[35] H. Irie, Y. Watanabe, K. Hashimoto, J. Phys. Chem. B 107 (2003) 5483.